Photosynthetic energy transfer: missing in action (detected spectroscopy)?

Ariba Javed[1,2]†, Julian Lüttig[1]†, Kateřina Charvátová[3], Stephanie E. Sanders[1], Rhiannon Willow[1], Muyi Zhang[1], Alastair T. Gardiner[4], Pavel Malý[3] and Jennifer P. Ogilvie[1,5]**

[1]Department of Physics, University of Michigan, 450 Church St, Ann Arbor MI 48109, USA

[2]Department of Materials Science and Engineering, University of Michigan, 2300 Hayward St., Ann Arbor, Michigan 48109-2136, USA

[3]Faculty of Mathematics and Physics, Charles University, Ke Karlovu 5, 121 16 Praha 2, Czech Republic

[4]Center Algatech, Institute of Microbiology, Czech Academy of Sciences, 37901 Třeboň, Czech Republic

[5]Department of Physics, University of Ottawa, 150 Louis-Pasteur Pvt, Ottawa, ON, Canada, K1N 6N5

AUTHOR INFORMATION

***Corresponding Authors**

Jennifer P. Ogilvie (experiment) and Pavel Malý (theory)

Email: jogilvie@umich.edu, pavel.maly@matfyz.cuni.cz

ABSTRACT

In recent years, action-detected ultrafast spectroscopies have gained popularity offering distinct advantages over their coherently-detected counterparts, such as spatially-resolved and *operando*

measurements with high sensitivity. However, there are also fundamental limitations connected to the process of signal generation in action-detected experiments. Here we perform fluorescence-detected two-dimensional electronic spectroscopy (F-2DES) of the light-harvesting II (LH2) complex from purple bacteria. We demonstrate that the B800-B850 energy transfer process in LH2 is weak but observable in F-2DES, unlike in coherently-detected 2DES where the energy transfer is visible with 100% contrast. We explain the weak signatures using a disordered excitonic model that accounts for experimental conditions. We further derive a general formula for the presence of excited-state signals in multichromophoric aggregates, dependent on the aggregate geometry, size, excitonic coupling and disorder. We find that the prominence of excited-state dynamics in action-detected spectroscopy offers a unique probe of excitonic delocalization in multichromophoric systems.

TOC GRAPHIC

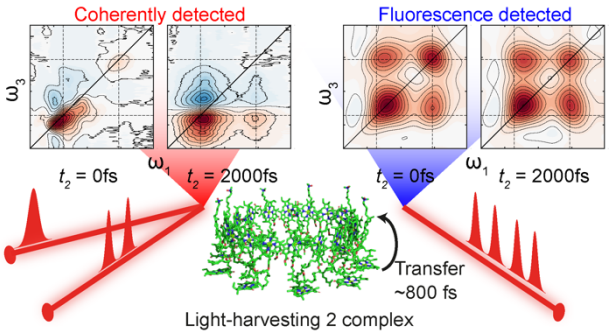

KEYWORDS ultrafast spectroscopy, energy transfer, photosynthesis

Two-dimensional electronic spectroscopy (2DES) has emerged as a powerful tool for studying electronic structure and dynamics in systems ranging from photosynthetic complexes to liquids

and solid-state materials [1, 2]. Both high temporal and spectral resolution can be achieved using Fourier transform 2DES, providing a significant advantage over lower dimensional approaches such as pump-probe spectroscopy. In addition, by expressing the signal as a 2D map correlating the excitation and detection frequencies, 2DES effectively decongests the spectral information available from conventional linear spectroscopies, enabling a better understanding of a wide variety of systems [3]. The most common implementation of 2DES utilizes a sequence of three time-delayed pulses that interact with the sample, generating a macroscopic third-order polarization that radiates a coherent signal field. Phase-matching is typically used to detect the coherent signal in a specific direction, requiring a sample volume greater than $\sim\lambda^3$ (where λ is the excitation wavelength) to attain the coherent build-up of a macroscopic signal [4]. This limits the use of coherent 2DES to studies of extended samples containing large numbers of molecules, making it ill-suited for single molecule studies and for combining with microscopy.

In recent years, motivated by the desire to make spatially-resolved measurements and to correlate optical excitation with a wide range of observables, action-detected variants of 2DES and pump-probe spectroscopy have been developed that employ a fully collinear geometry, relying on phase-cycling or phase-modulation to extract the signals of interest. These approaches overcome some of the limitations of coherent 2DES and have employed fluorescence [5-8], photocurrent [9-12], photoelectron [13-15], or photoion [16, 17] emission as experimental observables. Fluorescence-detection, in general, has enabled spatially-resolved measurements, while photocurrent, photoion and photoelectron detection have enabled *operando* device studies [18]. Numerous interesting systems including photosynthetic complexes [7, 8], atomic vapors [6, 14], molecular dimers [19, 20], dyads [21], semiconductor nanostructures [9, 11, 22, 23], as well as photovoltaic devices [12, 18, 24] have been studied using action-detected 2DES techniques. However, there are significant fundamental

differences between action-detected and coherent methods, and the interpretation of the spectra obtained from action-detected 2DES still remains an active research topic [25-31]. Studies comparing the spectra of coherently and action-detected measurements have been reported [20 32, 33], but to date there have been relatively few studies of excited-state dynamics with action-detected methods. In this work, we focus on fluorescence-detected 2DES (F-2DES) to highlight the similarities and differences between coherent and action-detected 2DES techniques for studying multichromophoric systems.

Compared to coherent 2DES (C-2DES), F-2DES adds a fourth pulse, projecting the third-order polarization onto an excited-state population of fourth order in the electric field. The resulting observable is an incoherent signal proportional to this excited-state population [6]. The difference between C-2DES and F-2DES arises due to the fourth pulse which leads to additional Liouville pathways [19, 27, 31]. The double-sided Feynman diagrams corresponding to these pathways are shown in *SI Appendix* Fig. S1, S2. In C-2DES, three contributions make up the spectra – the ground state bleach (GSB), stimulated emission (SE), and excited-state absorption (ESA), with the ESA pathway contributing with an opposite sign relative to the GSB and SE pathways. In F-2DES, in addition to GSB and SE pathways, two distinct and oppositely-signed ESA pathways exist, arising from emission upon excited to singly or doubly excited states. Depending on the relative quantum yields of the two excited states, the ESA pathways may partially or fully cancel, dramatically changing the appearance of F-2DES relative to C-2DES [19, 31, 34].

The measured excited-state populations in molecular systems typically have lifetimes on the scale of nanoseconds, orders of magnitude longer-lived than electronic coherences. This long-lasting signal generation provides additional opportunities for excited-state populations to interact and become correlated over longer timescales leading to partial or even full cancellation of the

ESA pathways. Second-order decay processes such as exciton-exciton annihilation (EEA), Auger recombination, photocarrier scattering, or nonlinearities in the detection can occur, contaminating the nonlinear signal and obscuring spectral dynamics [26, 29, 35, 36]. Using F-2DES, strong cross peaks at early waiting times have been reported in multichromophoric systems [7, 8], in contrast to the observations in C-2DES studies where weak or no cross peaks were present [37]. The appearance of cross peaks in F-2DES at early waiting times has been attributed to EEA [27, 31, 38] rather than to excitonic coupling as in C-2DES. F-2DES has revealed clear excited-state dynamics in small systems such as molecular dyads [19-21] and Rb atoms [17]. However, excited-state dynamics in extended multichromophoric systems have not been investigated, with the exception of weak kinetic signatures reported in photocurrent-detected 2DES studies of an organic photovoltaic device [10] and more recently in a biohybrid device incorporating photosystem I [39]. Recent theoretical and experimental work suggests that action-detected 2DES is poorly suited for this task [30, 39].

Here we study the light-harvesting II (LH2) complex from the purple bacterium *Rhodoblastus acidophilus (R. acidophilus)* using F-2DES to characterize its ability to resolve excited-state dynamics and probe excitonic structure in multichromophoric systems. The well-characterized structure and the extensive previous ultrafast studies [40-46] of LH2 make it an excellent model system for this purpose. It is comprised of two bacteriochlorophyll *a* (*BChl a)* rings, B800 and B850. The B800 ring consists of 9 monomeric *BChl a*, which are weakly coupled to each other giving rise to an absorption peak at ~800 nm. The B850 ring consists of 18 strongly coupled *BChl a* arranged in dimeric units, producing an absorption peak at ~850 nm. *SI Appendix* Fig. S5 shows the structure and orientation of the B800 and B850 rings in LH2 from *R. acidophilus* [47]. Many previous experimental studies have used C-2DES to probe the excited-state dynamics within LH2,

and have reported timescales ranging from ~700 fs to 1 ps for the B800 → B850 energy transfer [40-43]. Previous F-2DES studies of LH2 studies showed spectra at $t_2 = 0$ but did not report waiting-time-dependent F-2DES measurements [7, 8]. Here we present waiting-time-dependent F-2DES spectra of LH2 as well as the corresponding C-2DES data for comparison.

To gain insight into the F-2DES measurements of LH2 we formulate an excitonic model-based description of the F-2DES response. We derive a general dependence of the response on the excitonic structure, allowing us to quantify the effects of varying oscillator strength, excited-state population and excitonic delocalization on the prominence of the excited-state dynamics in the F-2DES spectra. The model successfully reproduces the measured LH2 F-2DES spectra and the weak B800-B850 energy-transfer signatures. We also examine other multichromophoric geometries, finding that the prominence of excited-state dynamics in F-2DES measurements is dependent upon both the excitonic state structure and excitonic delocalization. Our results demonstrate that F-2DES provides a sensitive probe of excitonic structure, while the prominence of excited-state dynamics reveals the exciton delocalization. Although we focus on F-2DES, our findings are applicable to all action-detected spectroscopies and thus demonstrate their unique potential to investigate multichromophoric systems.

The absorptive F-2DES spectra of LH2 are shown in Fig. 1 (top row) at waiting times t_2= 0 fs, 500 fs and 2 ps. The t_2 = 0 fs spectra show strong B800 and B850 diagonal peaks and prominent cross-peaks, consistent with previous work [7, 8]. By 500 fs, the relative amplitudes have changed, with the upper diagonal peak (UDP) from B800 losing intensity relative to the lower diagonal peak (LDP) from B850, and the ratio of cross-peak/diagonal peak amplitude increasing. Overall, the F-2DES spectra show little evolution in peak amplitudes or shapes as a function of waiting time, with the lower cross-peak (LCP), which corresponds to excitation of B800 and

detection of B850, showing the largest evolution in peak shape. The simulated F-2DES spectra are shown in Fig. 1 (middle row), displaying good agreement with the experimental measurements. In contrast to the F-2DES spectra, Fig. 1 (bottom row) shows the C-2DES spectra of LH2 at the same waiting times, revealing dramatic spectral evolution with increasing waiting time.

Fig. 2 shows the waiting-time dependence of the F-2DES diagonal and cross-peak amplitudes. The colored squares overlaid on the $t_2 = 0$ fs of the experimental and theoretical F-2DES spectra in Fig. 1 indicate the region over which the signal was integrated to obtain the kinetic traces shown in Fig. 2. All four peak amplitudes show a dramatic drop within the pulse overlap region, followed by very small amplitude changes within the first 2 ps. As we confirm by calculations, the rapid initial signal drop reflects coherence dephasing that we discuss further in the *SI Appendix*. The excitation dynamics are visible in the small changes that are more apparent in the panels below each kinetic trace, where the vertical scale is expanded. An exponential fit of the decay of the UDP amplitude reveals a time constant of 1480 ± 375 fs, and corresponds to a change of the signal amplitude of 4.4%. The LDP shows a rapid decay within the first ~200 fs followed by a roughly constant signal level. The upper cross-peak (UCP) shows little evolution during the first 2 ps aside from the initial amplitude drop. The LCP exhibits a small increase, which is fit to an exponential rise yielding a time constant of 1345 ± 575 fs, and corresponds to a signal rise of 6.2%. The corresponding waiting-time dependence of the C-2DES diagonal and cross-peak amplitudes are shown in *SI Appendix* Fig. S10. In contrast to F-2DES, the peak amplitude changes in C-2DES are much more apparent. In particular, the LCP, which is negligible at early waiting times, shows a clear exponential rise with a time constant of 825 ± 10 fs, amounting to ~100% of the cross-peak amplitude. Further details about the data fitting are provided in the *SI Appendix*.

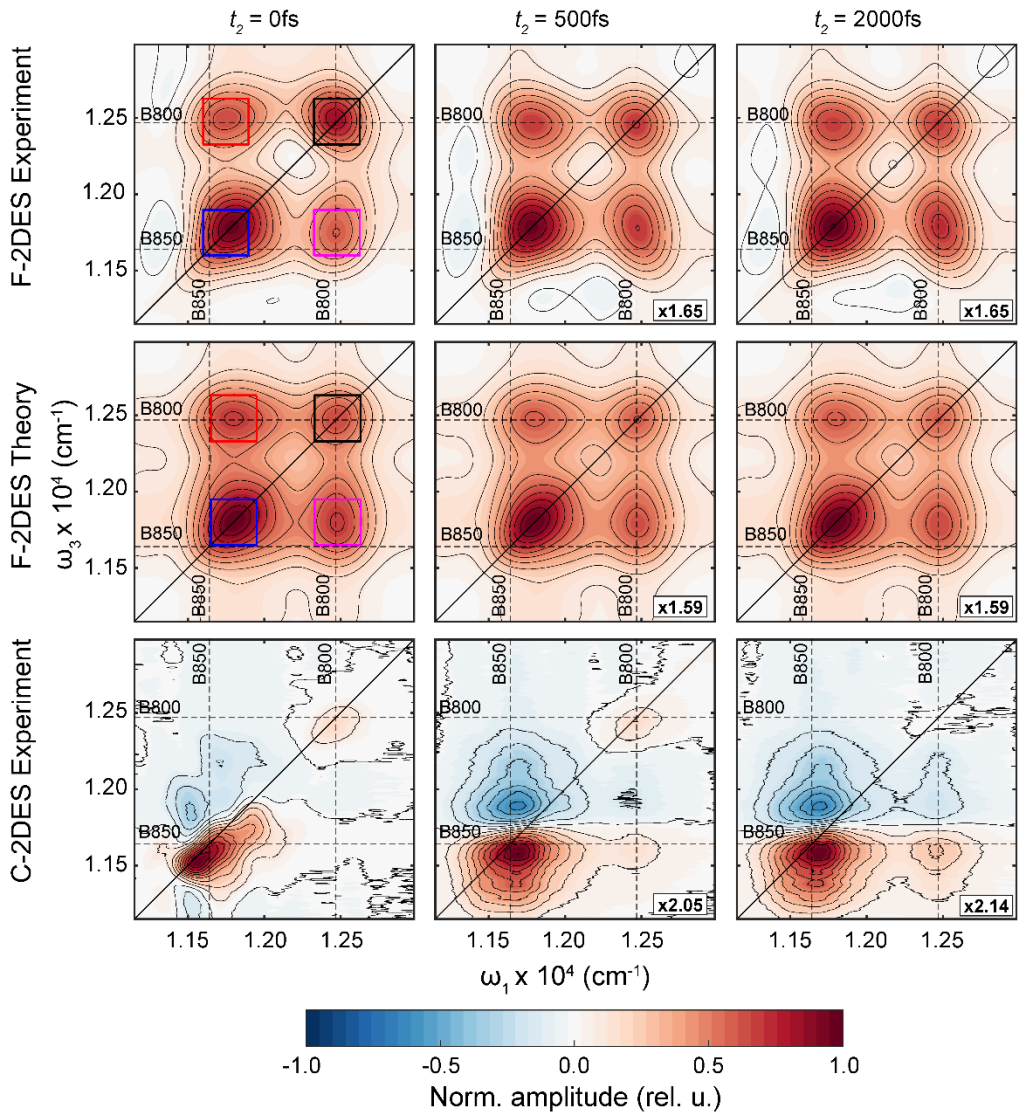

Fig. 1. Fluorescence and coherent-detected 2D spectra of LH2. Top row: F-2DES spectra of LH2 at waiting times t_2=0 fs, 500 fs and 2 ps. Middle row: Simulated F-2DES spectra of LH2 at waiting times t_2=0 fs, 500 fs and 2 ps. Bottom row: C-2DES spectra of LH2 at waiting times t_2=0 fs, 500 fs and 2 ps. The colored squares in the t_2=0 fs spectra in the top and middle row indicate the region over which the kinetic traces shown in Fig. 2 were averaged.

Bolzonello et al. recently presented theoretical studies of action-detected 2DES of molecular assemblies [30]. They find that when the output signal intensity is not proportional to the number of

excitations generated in the system, *e.g.* because of EEA, the visibility of excited-state dynamics is reduced as the number of chromophores increases. When the EEA is efficient, as is the typical case of molecular aggregates such as LH2, the intensity of excited-state dynamics in the signal is given by the ratio of the SE to GSB contribution. Based on a combinatoric argument, the SE/GSB ratio scales as $1/N$ for an aggregate of N identical molecules. Here we test the applicability of their combinatoric approach to LH2. In Fig. 3 we present double-sided Feynman diagrams that depict the signals that contribute to the LCP and UDP of the F-2DES spectrum of LH2. These represent the features sensitive to the B800-B850 energy transfer. Only the SE and GSB pathways are present since the two oppositely-signed ESA contributions (shown in *SI Appendix* Fig. S1, S2) cancel [21]. We note that the ESA cancellation in molecular aggregates is determined by the efficiency of EEA and the quantum yield of higher excited states of the constituent molecules relative to that of their lowest excited state. The EEA efficiency in small, dense aggregates such as LH2 typically reaches unity. According to the Kasha-Vavilov rule [48], for typical molecules the fluorescence quantum yield is independent of the excitation wavelength, as verified for BChl a and chlorophyll a [49]. The ESA cancellation can thus be expected for most typical molecular aggregates. For the simple combinatoric argument we consider the system to be weakly coupled, such that the

site basis is appropriate, with the number of pigments on the B800 and B850 rings given by N_{800} = 9 and N_{850} = 18 respectively. We later discuss the implications of excitonic coupling.

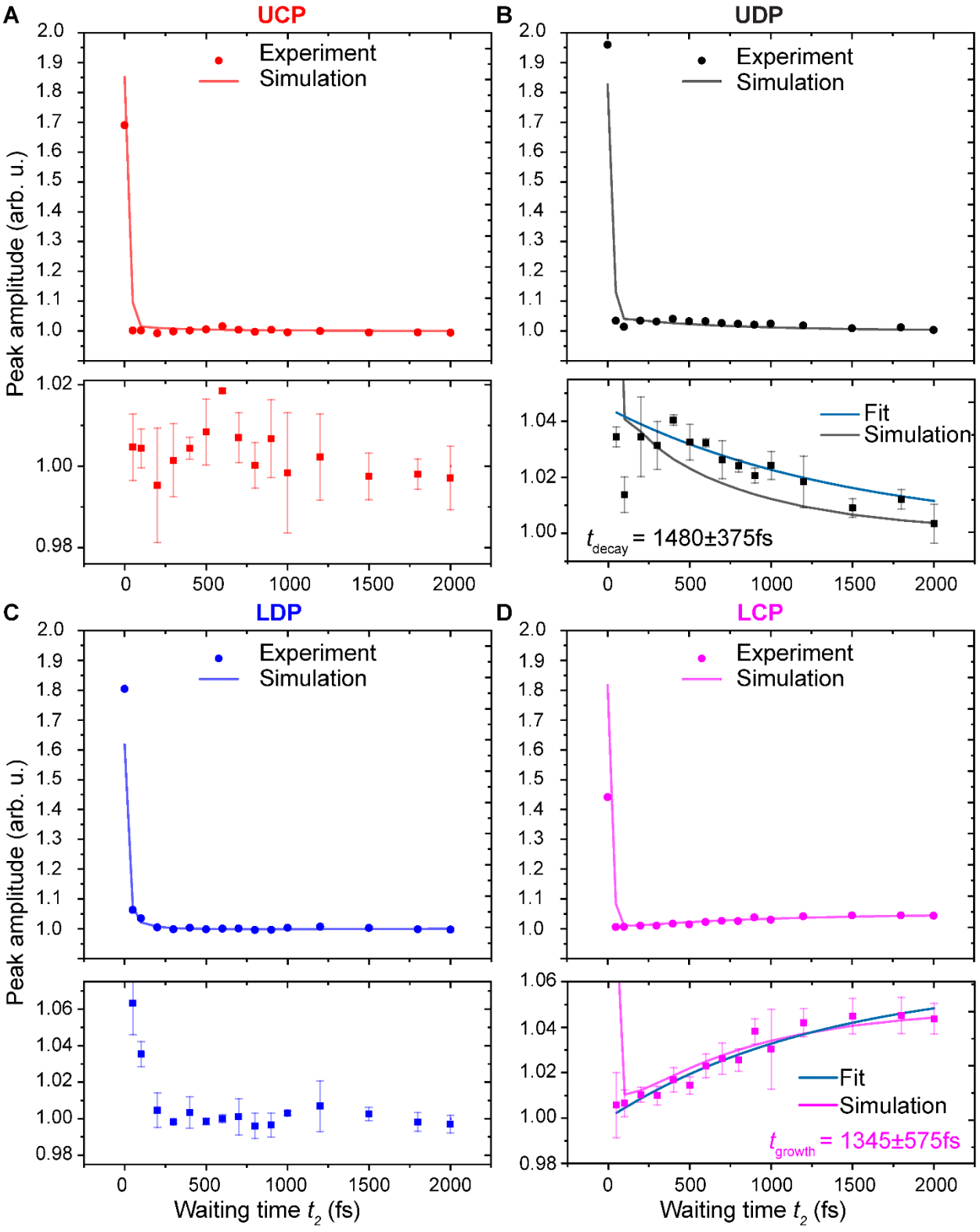

Fig. 2. Kinetic traces for different peak positions. Experimental and simulated kinetic traces as a function of waiting time t_2 at (**A**) the upper cross peak (UCP), (**B**) upper diagonal peak (UDP), (**C**) lower diagonal peak (LDP) and (**D**) lower cross peak (LCP) locations, obtained by averaging over the regions indicated by colored squares in Fig. 1. Below each kinetic trace, an expanded vertical scale excludes the t_2 = 0 fs peak to more clearly visualize the weak kinetic signatures. Error bars are derived from three distinct measurements. Exponential fits to the UDP and lower cross-peak LCP are also shown, yielding SE_{B800}/GSB_{B800} = 4.4% and SE_{B850}/GSB_{B850} = 6.2% respectively. The UCP and LDP were normalized such that the peak amplitude at long waiting times (>1ps) was 1 on average. The traces were normalized to the GSB contribution as further described in the *SI Appendix.*

The LCP can be described by diagrams in which the first pulse pair interacts with the i^{th} pigment on the B800 ring, while the second pulse pair interacts with the j^{th} pigment on B850 ring as shown in Fig. 3A. The SE pathways clearly exhibit interband energy transfer from B800 to B850 during the waiting time t_2, resulting in a rise in the LCP amplitude. In addition to the SE pathways, an even larger number of GSB pathways exist that contribute to the LCP. The number of SE pathways is N_{B800} = 9. In contrast, the number of GSB pathways is N_{B800} * N_{B850} = 9*18 = 162. If all pathways were equally weighted, the fraction of signal showing kinetics would be given by SE/GSB = 9/162 = 1/18 = 5.6% of the signal. This appears to be in quite good agreement with the data shown in Fig. 2D in which the exponential rise due to B800-B850 energy transfer constitutes ~6.2% of the signal.

A similar argument can be made for the UDP, which has contributions from the GSB and SE pathways shown in Fig. 3B. In these pathways, the initial pulse pair interacts with the i^{th} B800

pigment, while the second pulse pair interacts with the k^{th} B800 pigment. The spectroscopic signatures of interband energy transfer, i.e., a rise of the LCP and a decay of the UDP, are connected to all the SE pathways since only these pathways include an excited-state population during the waiting time t_2. The, intraband energy transfer can occur during waiting time t_2 as well. However, stimulated emission must occur from whichever pigment is in the excited state at the time of the third light-matter interaction (the k^{th} pigment), making the total number of SE pathways equal to $N_{B800} = 9$. In contrast, there are $N_{B800} * N_{B800} = 81$ GSB pathways including the correlation of all B800 transitions. Assuming equal contributions of all pathways, for the UDP, the ratio of SE/GSB = 9/81 = 1/9 = 11%. This does not agree with the data, which show a considerably lower prominence of excited-state kinetics of ~4.4% derived from the exponential fit to the UDP in Fig. 2B.

From the pathway analysis above, it is clear that the excited-state dynamics is reflected in the SE contribution, visible as the UDP decay and LCP rise with the energy transfer between the rings. This transfer makes it possible to distinguish the spectrally identical SE and GSB contributions. Since only the number of pathways figures into the combinatoric argument, the disagreement with experiment suggests that the assumption of equal weight of all pathways is not valid. This implies different transition strengths in aggregates composed of the same molecules (*BChl a* in case of LH2), indicative of excitonic effects such as delocalization.

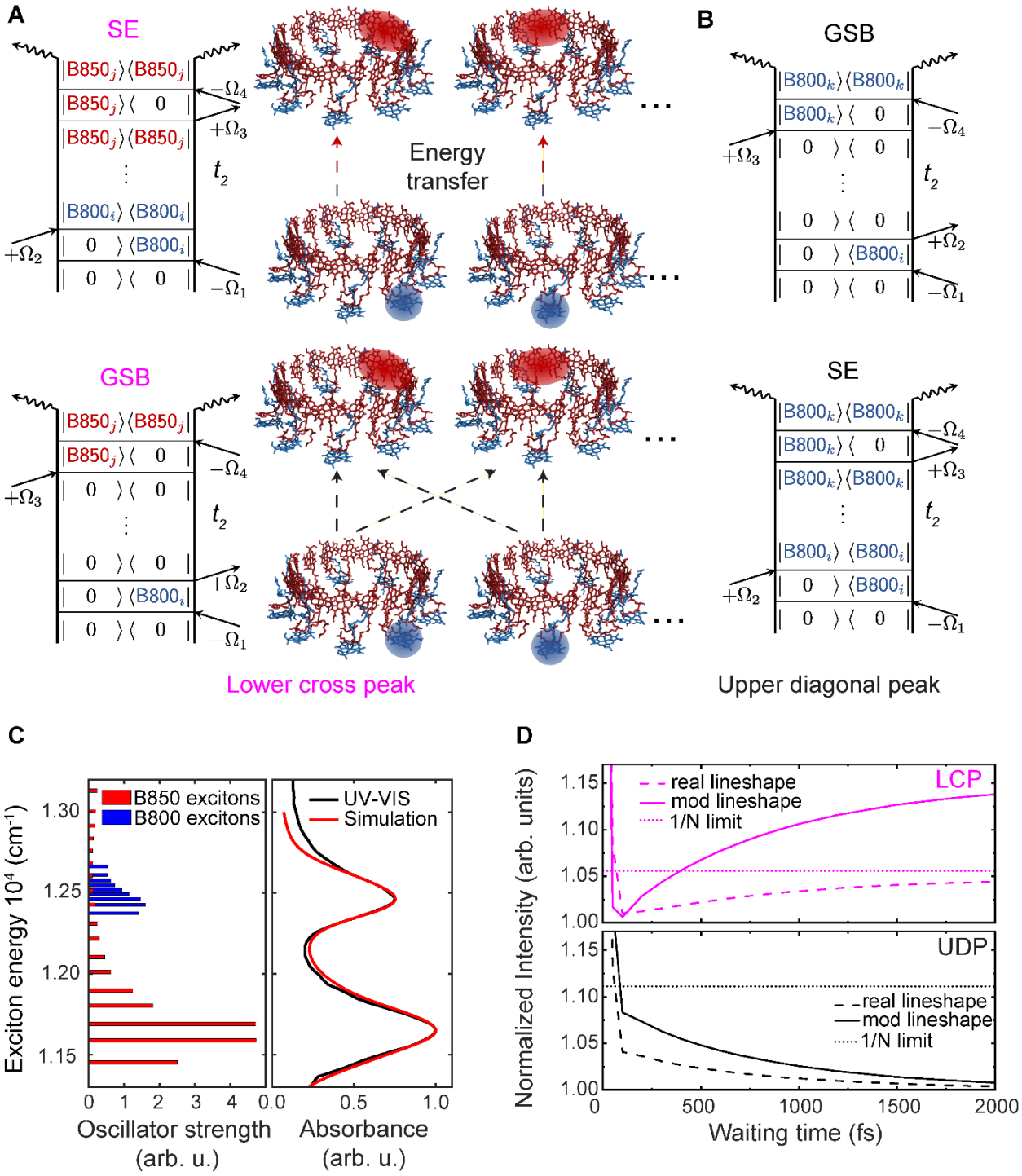

Fig. 3. Signatures of energy transfer in F-2DES. (**A**) Double-sided Feynman diagrams depicting the signals that contribute to the lower cross peak (LCP) which exhibits B800 to B850 energy transfer (ET) during waiting time t_2. The structure was taken from the RSCB protein databank [2FKW]. [50] (**B**) Double-sided Feynman diagrams depicting the signals that contribute to the upper

diagonal peak (from B800). (**C**) Excitonic model of LH2, showing the energies and oscillator strengths of the excitonic states of the B800 and B850 bands (left). Experimental (black) and simulated (red) linear absorption spectrum of LH2 (right). (**D**) Simulated t_2-dependent kinetic traces of the lower cross peak (upper panel) and upper diagonal peak (lower panel) using realistic lineshapes that take into account the finite laser spectrum bandwidth (dashed) and modified lineshapes that would be acquired with a flat laser spectrum (solid). The traces were normalized to the GSB contribution as further described in the *SI Appendix*. The $1/N$ limits (dotted) are plotted at the $1/N$ value above 1 for the LCP/UDP.

To understand the experimental F-2DES data and the effect of excitonic structure, we performed simulations to analyze the nonlinear response using Liouville-space pathways and account for the excitonic nature of LH2. As before, we assume, due to EEA, that the spectra contain only two types of contribution: GSB and SE, of which only the latter reports on the excited-state dynamics. We employ a standard disordered excitonic model for LH2 [51-53] as described in the Methods section and in detail in the *SI Appendix*. Diagonalization of the system Hamiltonian yields the excitonic state structure shown in Fig. 3C. In the B800 ring, the excitons are mostly localized, with similar oscillator strengths. In contrast, in the B850 ring a few bright states dominate the absorption band, while the rest have small oscillator strength and higher energy. The linear absorption (Fig. 3C) and F-2DES spectra (Fig. 1 Middle row) were calculated by summing all the appropriate response pathways (see *SI Appendix*). To better represent the experiment, the calculated F-2DES spectra of LH2 were additionally multiplied by the laser spectrum along both frequency axes and convolved with the Fourier transform of the time-domain filter function used in the experimental data processing. As can be seen from Fig. 1, the

agreement of the theory and experiment is excellent. Upon applying the same analysis that we used for the experimental data, we extract the apparent SE/GSB ratios of the B800 and B850 manifolds directly from the kinetics of the integrated UDP and LCP as shown in Fig 2B and D respectively. We obtain contrasts of SE/GSB = 4.1% and SE/GSB = 4.8% from the UDP and LCP, in good agreement with the experimental values of 4.4% and 6.2% respectively. This agreement demonstrates that the combination of excitonic effects and the influence of finite laser spectra on the measured line-shapes can explain the observed presence of excited-state dynamics in F-2DES measurements.

To disentangle the effects of excitonic structure and the finite laser spectrum we calculated the F-2DES spectra with spectrally flat pulses. In Figure S14 we show that the finite laser spectrum effectively pulls the diagonal and cross-peaks together, making their individual kinetics more difficult to separate. Fig. 3D compares the excited-state kinetics of the UDP decay and LCP rise calculated with the finite laser bandwidth (dashed lines), flat laser spectrum (solid lines), and the $1/N$ limit that assumes identical sites and perfect distinction of the SE and GSB. Clearly, the finite bandwidth increases the peak overlap, decreasing the apparent SE/GSB ratio and thus the excited-state dynamics visibility. Crucially, as seen from the LCP rise for the flat spectra, the excitonic effects can enhance the excited-state dynamics far beyond what is expected from the number of pigments. To gain insight into this effect, we consider a generic aggregate of N coupled two-level systems. The response pathways can be separated into those with excitonic population and inter-exciton coherence in t_2. The inter-excitonic coherence dephases rapidly and leads to the initial signal drop which is not relevant for the excitation transfer. We thus consider only the population pathways. The ratio between the spectrally-integrated SE and GSB in the absorptive F-2DES spectra can be expressed as

$$\frac{\mathrm{SE}}{\mathrm{GSB}} = \frac{\sum_{i,j=1}^{N} \langle \mu_i \mu_i \mu_j \mu_j \rangle U_{ji}(t_2)}{\sum_{i,j=1}^{N} \langle \mu_i \mu_i \mu_j \mu_j \rangle}. \quad (1)$$

Here, μ_i is the transition dipole moment of the excitonic state i, and $U_{ji}(t_2)$ is the population propagator in the waiting time t_2, i.e., the conditional probability that, provided the excitation started in state i, it will be in state j after time t_2 has passed. The orientational averaging is denoted by $\langle\rangle$. The F-2DES spectra of LH2 were measured and calculated with all-parallel pulse polarizations and thus contains a weak anisotropy contribution. Here, to isolate the population dynamics only, we will consider the isotropic signal acquired under the so-called magic angle between the polarization of the first and second pulse pairs, for which $\langle \mu_i \mu_i \mu_j \mu_j \rangle_{\mathrm{m.a.}} = \frac{1}{9} |\mu_i|^2 |\mu_j|^2$. There are two limits under which the SE/GSB ratio reduces to the combinatoric result of Bolzonello et al. [30]: a uniform population of all states regardless of the initial state (*e.g.,* iso-energetic landscape), $U_{ji}(t_2) = \frac{1}{N} \forall i,j$, and all states with the same oscillator strength $|\mu_i|^2 = |\mu|^2 \forall_i$. For these cases, Eq. (1) for the ratio reduces to

$$\left(\frac{\mathrm{SE}}{\mathrm{GSB}}\right)_{\text{uniform population}} = \left(\frac{\mathrm{SE}}{\mathrm{GSB}}\right)_{\text{same oscillator strength}}$$

$$= \frac{1}{N}. \quad (2)$$

However, none of these situations strictly applies to real aggregates. An interesting case is that of (quasi)equilibration within the excitonic manifold, for which we have $U_{ji}(t_2) = P_j^{eq} \forall i$. In this case, the $\sum_i |\mu_i|^2$ can be factored out and the SE/GSB ratio becomes

$$\left(\frac{\mathrm{SE}}{\mathrm{GSB}}\right)_{\text{equilibrated}} = \frac{\sum_{j=1}^{N} |\mu_j|^2 P_j^{\mathrm{eq}}}{\sum_{j=1}^{N} |\mu_j|^2}. \quad (3)$$

In the ratio, the sum of the oscillator strengths (GSB) is compared to the same sum weighted by the populations. At thermal equilibrium at temperature T, the population of the excitonic states are $P_j^{eq} = \exp\left(-{}^{\epsilon_j}/_{k_B T}\right) \left(\sum_{k=1}^{N} \exp\left(-{}^{\epsilon_k}/_{k_B T}\right)\right)^{-1}$ where ϵ_j are the state energies. Depending on the

excitonic state structure (energies, oscillator strength, delocalization), the SE/GSB ratio can thus be larger or smaller than 1/*N*.

Eqs. (1)-(3) are very simple and connect the static properties of the excitonic manifolds, without considering dynamics or line shapes, to the SE/GSB ratio that is observable as the weak dynamics in F-2DES spectra. To verify that the extracted SE/GSB ratio can indeed be inferred from the excitonic structure in realistic systems, we calculated the F-2DES spectra of various aggregates, as described in the SI. In F-2DES, the SE can be distinguished from GSB either by its spectrum or kinetics. In excitonic manifolds with many states, this can prove to be very difficult due to large spectral overlap and small SE/GSB ratio. This is the case of the individual LH2 rings as well, both of which have broad, featureless spectra. Fortunately, the excitation transfer between the rings allows us to distinguish the excited-state dynamics from the constant GSB contribution. We thus also construct our test aggregates with two spectrally distinct manifolds. For aggregates of varying geometries, sizes and excitonic delocalization, we have extracted the SE/GSB ratios and compared them to the results of Eq. (3), finding excellent agreement (see *SI Appendix*). This indicates that it is indeed the static excitonic state structure that dictates the presence of excited-state dynamics. These expressions apply to any aggregate that features distinct excitonic manifolds with rapid intra-manifold equilibration and slow inter-manifold energy transfer. One extreme case would be a perfect J aggregate for which all oscillator strength is in the lowest-energy state, leading to $\left(\frac{\mathrm{SE}}{\mathrm{GSB}}\right)_{\mathrm{J-agg}} \to 1$. The opposite extreme case is a perfect H aggregate in which only the highest-energy state is bright, leading to a vanishing SE in the excited-state equilibrium and $\left(\frac{\mathrm{SE}}{\mathrm{GSB}}\right)_{\mathrm{H-agg}} \to 0$. In general, the ratio will be somewhere between these two extremes, depending on the aggregate geometry, electronic coupling, energetic disorder and the excitonic delocalization (see Fig. 4A). In the case of the linear J/H aggregate, the SE/GSB ratio monotonously increases/decreases with

the excitonic coupling relative to energetic disorder, correlating with the excitonic delocalization. In these aggregates, the SE/GSB ratio thus directly reports on the excitonic delocalization. A slightly more complex example is a circular aggregate in which the dipole moments are oriented tangentially to the circle. In a large circle (small coupling) the dominating interaction is between nearest neighbors, and the aggregate has J-type character, with the SE/GSB ratio increasing with delocalization. When decreasing the circle size (increasing coupling), the ratio reaches its maximum and then starts to decrease, signifying the transition to predominantly H-type behavior.

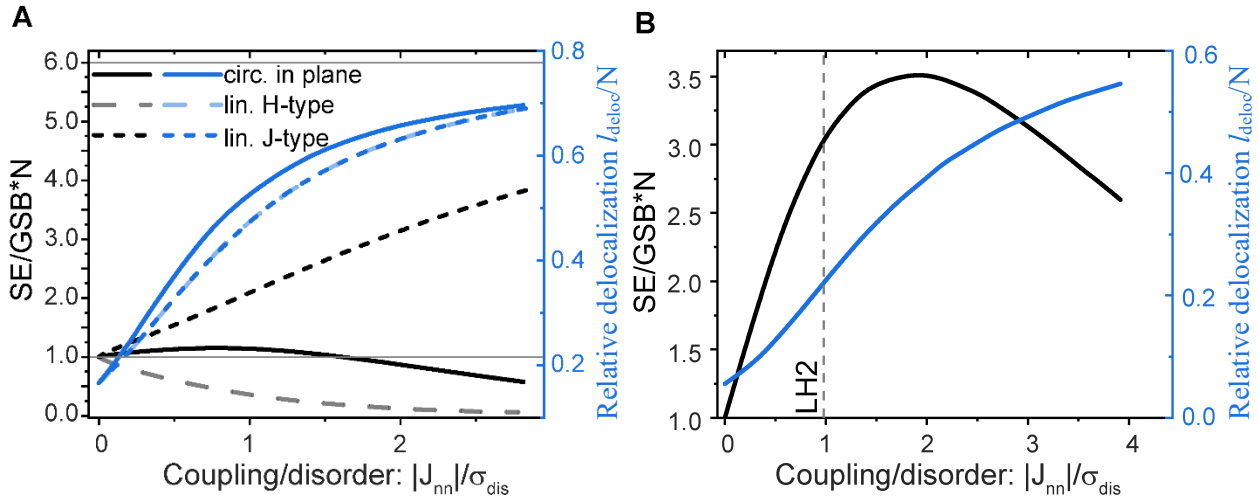

Fig. 4. Effect of delocalization on the signatures of energy transfer in F-2DES. (**A**) Dependence of the SE/GSB ratio on the excitonic delocalization for different types of molecular aggregates. Here the electronic coupling is characterized by the nearest-neighbour coupling J_{nn}, while σ_{dis} characterizes the Gaussian disorder (mean square deviation). The delocalization length l_{deloc} (blue) is calculated as described in the Methods section. Thin, gray lines at 1 and 6 are the $1/N$ value for identical molecules and the maximum ratio for a perfect J-aggregate with 6 monomers. (**B**) Dependence of the SE/GSB ratio on the excitonic delocalization for the LH2 B850

ring. The dotted line indicates the $|J_{nn}|/\sigma_{dis}$ used in the F-2DES simulations, yielding a SE/GSB ratio of ~3 times larger than the 1/*N* limit.

Having discussed the general aggregates, we briefly return to LH2 to understand the role of excitonic coupling and delocalization in the observed dynamics. Fig. 4B depicts the dependence of the SE/GSB ratio on the excitonic delocalization for the LH2 B850 ring, in which both the electronic coupling and energetic disorder are relatively strong, leading to a significant excitonic delocalization and more complex state structure [53]. At the same time, the equilibration within the B850 manifold is much faster than the B800→B850 transfer, so that Eq. (3) applies. To include the population transfer, Eq. (3) can be augmented as

$$\left(\frac{\mathrm{SE}}{\mathrm{GSB}}\right)_{\mathrm{B800}} = \frac{\sum_{k=1}^{9} P_k^{eq} \left|\mu_{B800_k}\right|^2}{\sum_{k=1}^{9} \left|\mu_{B800_k}\right|^2} e^{-k_{B800\rightarrow B850} t_2} \qquad (4)$$

for the B800 ring, and

$$\left(\frac{\mathrm{SE}}{\mathrm{GSB}}\right)_{\mathrm{B850}} = \frac{\sum_{j=1}^{18} P_j^{eq} \left|\mu_{B850_j}\right|^2}{\sum_{j=1}^{18} \left|\mu_{B850_j}\right|^2} \mathrm{X}$$

$$(1 - e^{-k_{B800\rightarrow B850} t_2}). \qquad (5)$$

for the B850 ring. These expressions formalize the connection to the UDP decay and LCP rise observed in the experimental F-2DES data.

The geometry of the LH2 B850 18-*BChl a* ring is similar to that of the circular aggregate, leading to an analogous non-monotonous SE/GSB ratio dependence. For realistic LH2 parameters, the electronic nearest-neighbor coupling and energetic disorder are of a very similar magnitude which results in the lowest-energy states carrying most of the oscillator strength. This places the SE/GSB ratio close to its maximum in Fig. 4B. We thus have from just the excitonic structure, the rise of the LCP is SE_{B850}/GSB_{B850} = 17% (18% for all-parallel), which is ~3 times larger than 1/*N*=1/18 limit (5.5%) as well as the extracted experimental value of 6.2%. In the B800 ring the

coupling and thus delocalization is much weaker, giving SE_{B800}/GSB_{B800} = 13% (11% for all-parallel pulse polarizations). This matches the $1/N$=1/9 (11%) value for independent sites, but is again larger than the experimental value of 4.4%. As in the experiment, the SE/GSB ratio is about 1.5 times larger in the B850 ring (seen in the LCP) than in the B800 ring (seen in the UDP). The values are, however, larger than the experimental ones, highlighting the importance of including realistic lineshapes and the effects of finite laser bandwidth. A summary of the various SE/GSB ratios extracted from the different calculations is given in *SI Appendix* Table S1 for easy comparison with the experimentally determined ratios.

The growing popularity of action-detected 2D spectroscopies motivates an in-depth analysis of their potential for probing excited-state dynamics in molecular systems. While F-2DES has revealed excited-state dynamics in molecular dyads [19-21] and Rb atoms [17], recent work [30] raises doubts about the extent to which excited-state dynamics are visible in larger molecular aggregates. Using LH2 as a model system, our experimental data clearly demonstrates that F-2DES of LH2 shows weak but distinct spectral evolution as a function of the waiting time, in stark contrast to C-2DES (see Fig. 1). In particular, the kinetics of energy transfer from B800 to B850 are difficult to discern in F-2DES, constituting a ~6.2% change in the signal level of the LCP, compared to ~100% in C-2DES. The rise in the LCP in the F-2DES data occurs with a time constant of 1345 ± 575 fs, consistent with previous reports of the B800-B850 energy transfer time [54] and with our C-2DES measurement of 825 ± 10 fs. The substantially smaller relative kinetic signals in F-2DES compared to C-2DES means that high signal-to-noise ratio is required for resolving LH2 energy transfer kinetics with F-2DES. For observing energy transfer in LH2, C-2DES offers a clear advantage

over F-2DES. However, the strength of the excited-state signatures in F-2DES carry important information about the excitonic structure as discussed below.

In order to understand the origin of the kinetic signatures in the F-DES spectra of LH2, we first examined the LH2 signals in the context of the combinatoric argument presented by Bolzonello et al. [30]. At first glance, the experimentally extracted SE_{B850}/GSB_{B850} of 6.2% appears in good agreement with the estimate of 5.6% obtained from the $1/N$ limit for the LCP. This fortuitous agreement incorrectly suggests an absence of excitonic delocalization in the B850 band. One would expect even better agreement with the $1/N$ limit for the B800 band due to its considerably weaker coupling in comparison to B850. Here we find that the $1/N$ limit fails, predicting SE_{B800}/GSB_{B800} = 11% for the UDP, greatly exceeding the experimental value of 4.4%. Seeking better agreement with the experimental data we simulated the F-2DES spectra based on an excitonic model for LH2, using parameters consistent with previous work. Our F-2DES simulations showed weaker dynamic signatures than expected based strictly on the excitonic model of LH2. We attributed this to the insufficient separation of the broad B800 and B850 peaks in the F-2DES spectrum, and the effects of finite laser bandwidth. Taking both the laser spectrum and peak overlap into account we were able to obtain SE/GSB ratios in good agreement with the F-2DES measurements. The SE/GSB value reports on the interplay of excitonic coupling and disorder, allowing us to infer the delocalization within the B850 ring (Fig. 3C) to be about 3.5 to 4 *BChl*s, in agreement with previous studies [52, 55, 56].

Through simulation we explored other molecular aggregate geometries, showing that the relative prominence of the excited-state dynamics is determined by the structure of the excitonic state manifold. Dependent on the aggregate geometry, the relative contribution of the excited-state dynamics can be greatly enhanced or suppressed. When the geometry of the system is known,

there is a clear relation between the SE/GSB ratio and excitonic delocalization. This allows excitonic delocalization to be inferred within dense excitonic manifolds. We note that this is a unique feature of F-2DES which is distinct from C-2DES, for which coherent artifacts near time zero and ESA signals that are oppositely-signed from GSB and SE complicate the determination of excitonic coupling and delocalization [20, 57]. While it might be difficult to distinguish the SE from GSB within the manifold by itself, the presence of an additional, spectrally separated manifold connected by slow excitation transfer is sufficient to make the SE visible. We note that future experimental advances, such as time-gating the fluorescence signal in F-2DES [31, 38] could allow for isolation of the SE signals, as could the recently-proposed 2D-FLEX method [58].

Given the difficulty in observing excited-state dynamics in multichromophoric systems with F-2DES, the question arises as to what systems and questions are better-suited to action-detected spectroscopies compared to their coherent counterparts. Action-detected spectroscopy combines several advantages such as absence of nonresonant contributions, spatially resolution and high sensitivity down to the single molecule level [59]. Photocurrent-based 2DES measurements of solar cell materials have shown wide variability in their sensitivity to excited-state dynamics between semiconductor-nanocrystal [9], perovskite [35] and organic samples [10]. The work of Bolzonello et al. [30] suggests that the ability of action-based 2DES to resolve excited-state dynamics decreases with system size, as predicted by their $1/N$ limit. They point out that "N should be identified with the number of absorbing states rather than the number of independent chromophores". Eq. (3) is consistent with this idea, showing that the excitonic structure reweights the relative contributions of the states, showing that in the case of strong delocalization, it is possible to significantly beat the $1/N$ limit. Thus, characterizing the SE/GSB ratio provides direct information about excitonic delocalization, a clear benefit of action-detected measurements.

Remarkably, this works for dense excitonic manifolds as well, as long as the SE can be distinguished, for example by its dynamics as in LH2. An interesting effect occurs if large multichromophoric systems are connected to a smaller system containing only a few pigments. Our analysis suggests that energy transfer to the smaller system might be still observable in the cross-peak dynamics since the SE/GSB ratio depends only on the structure of final excitonic manifold [see Eq. (3)]. One particular system might be the Heliobacterial reaction center in which the antenna and the core of the reaction center can be spectrally separated [60]. In addition, probing the excitonic structure via F-2DES might be particularly informative for systems with broad ESA signals such as photosynthetic reaction centers. Separated from their antenna complexes, these systems contain a small number of pigments. Understanding their excitonic structure in the low energy Q_y region is an outstanding challenge due to a combination of disorder and spectral overlap of the constituent pigments. Attempts to leverage distinct Q_x signatures of the pigments to untangle the Q_y excitonic structure have been complicated by the broadband ESA signals in the Q_x region [61]. Should the oppositely-signed ESA pathways in F-2DES cancel in such systems as they do in LH2, broadband F-2DES measurements may offer advantages over C-2DES for revealing excitonic structure.

The LH2 samples from *Rbl. acidophilus* were prepared following established protocols [62] that are described in detail in the *SI Appendix*. Our experimental setup for the F-2DES measurements is based on the acousto-optic phase modulation and lock-in detection scheme first demonstrated by Marcus and co-workers [6, 63], and used previously by us [7, 21]. We describe our current implementation in detail in the *SI Appendix*. The pulse energies used were 5.5 pJ per pulse with spot sizes of 16 μm, exciting ~10% of the sample at each laser shot. Samples were flowed at ~75 mL/min to reduce photobleaching effects. The t_1 and t delays were scanned from 0 to 91 fs,

in steps of 7 fs, while t_2 was scanned from 0 to 2000 fs. A lock-in time constant of 100 ms was used in the measurements and the signal at each combination of the three delays was averaged over 60 acquisitions (8 min per t_2 delay). The C-2DES measurements were made in the pump-probe geometry as reported previously [64]. The pump pulses had a total pulse energy of 7.3 nJ and were focused to 190 μm at the sample position, whereas the probe pulse had a pulse energy of 2.5 nJ and was focused to 180 μm. The t_1 delay was scanned from 0 to 180 fs, in steps of 5 fs, in the partially rotating frame with 0-π phase cycling. For the B800-B850 energy transfer kinetics, t_2 was scanned from -100 to 5000 fs in 100 fs steps. Each t_2 spectrum was collected in ~1.5 minutes, requiring ~90,000 total laser shots. Further details on the C-2DES implementation are in the *SI Appendix*.

The excitonic model of LH2 was constructed as follows (additional details in the *SI Appendix*). Using the structure from the RSCB protein databank [2FKW] [50], we calculate the electronic coupling via the dipole-dipole approximation. We assume identical site energies for the B800 band, and *BChl a* dimers in the B850 band [65], with Gaussian energetic disorder three-times stronger in the B850 band, reflecting possible charge-transfer character [66]. The static excitonic structure is depicted in Fig. 3A. The excitonic delocalization can be calculated as $l_{\mathrm{deloc}} = N\left(\sum_{i,n=1}^{N}\left|c_n^i\right|^4\right)^{-1}$, where c_n^i are the coefficients of the transformation from the site basis (index n) to the excitonic basis (index i), where N=9 for the B800 ring and N=18 for the B850 ring. We describe the vibrational bath using a 3-component Brownian oscillator model, and intra-manifold population relaxation rates as well as coherence dephasing are calculated using Redfield theory. The excitonic lineshapes are calculated by a cumulant expansion using the same spectral density, considering exchange-narrowing and relaxation-induced broadening. For faster calculations in the frequency domain, the lineshape was fit to a Lorentzian. The waiting time propagator $U(t_2)$ was calculated

using the secular approximation and matrix exponential, with the excitation transfer between the rings described by a site-independent rate with time constant of 830 fs.

ASSOCIATED CONTENT

Supporting Information: Photosynthetic energy transfer: missing in action (detected spectroscopy)? (PDF)

For instructions on what should be included in the Supporting Information as well as how to prepare this material for publications, refer to the journal's Instructions for Authors.

The following files are available free of charge.

brief description (file type, i.e., PDF)

brief description (file type, i.e., PDF)

ACKNOWLEDGMENTS

Funding:

National Science Foundation grant #PHY-1914608 (S.E.S., J.P.O)

Air Force Office of Scientific Research Biophysics program FA9550-18-1-0343 (A. J.)

Air Force Office of Scientific Research Biophysics program FA9550-21-1-0098 (J. L.)

U.S. Department of Energy DE-SC0016384 (R.W, M. Z.)

Human Frontier Science Program grant LT0056/2024-C (J. L.)

Author contributions:

† These authors contributed equally to the work

Conceptualization: AJ, JL, SES, PM, JPO

Methodology: AG, PM, JPO

Investigation: AJ, JL, SES, KC, RW, MZ, ATG, PM, JPO

Visualization: AJ, JL, SES, PM, JPO

Supervision: PM, JPO

Writing—original draft: AJ, JL, SES, ATG, PM, JPO

Writing—review & editing: AJ, JL, SES, KC, ATG, PM, JPO

REFERENCES

1. Mukamel, S.; Abramavicius, D.; Yang, L. J.; Zhuang, W.; Schweigert, I. V.; Voronine, D. V., Coherent Multidimensional Optical Probes for Electron Correlations and Exciton Dynamics: From Nmr to X-Rays. *Accounts Of Chemical Research* **2009,** *42* (4), 553-562.

2. Ogilvie, J. P.; Kubarych, K. J., Multidimensional Electronic and Vibrational Spectroscopy: An Ultrafast Probe of Molecular Relaxation and Reaction Dynamics. *Advances in Atomic, Molecular, and Optical Physics* **2009,** *57*, 249-321.

3. Jonas, D. M., Two-Dimensional Femtosecond Spectroscopy. *Annual Review of Physical Chemistry* **2003,** *54*, 425-463.

4. Tian, P.; Keusters, D.; Suzaki, Y.; Warren, W. S., Femtosecond Phase-Coherent Two-Dimensional Spectroscopy. *Science* **2003,** *300* (5625), 1553-1555.

5. Wagner, W.; Li, C. Q.; Semmlow, J.; Warren, W. S., Rapid Phase-Cycled Two-Dimensional Optical Spectroscopy in Fluorescence and Transmission Mode. *Optics Express* **2005,** *13* (10), 3697-3706.

6. Tekavec, P. F.; Lott, G. A.; Marcus, A. H., Fluorescence-Detected Two-Dimensional Electronic Coherence Spectroscopy by Acousto-Optic Phase Modulation. *The Journal of chemical physics* **2007,** *127* (21).

7. Tiwari, V.; Matutes, Y. A.; Gardiner, A. T.; Jansen, T. L. C.; Cogdell, R. J.; Ogilvie, J. P., Spatially-Resolved Fluorescence-Detected Two-Dimensional Electronic Spectroscopy Probes Varying Excitonic Structure in Photosynthetic Bacteria. *Nature Communications* **2018,** *9* (1), 4219.

8. Karki, K. J.; Chen, J.; Sakurai, A.; Shi, Q.; Gardiner, A. T.; Kühn, O.; Cogdell, R. J.; Pullerits, T., Before Förster. Initial Excitation in Photosynthetic Light Harvesting. *Chemical science* **2019,** *10* (34), 7923-7928.

9. Karki, K. J.; Widom, J. R.; Seibt, J.; Moody, I.; Lonergan, M. C.; Pullerits, T.; Marcus, A. H., Coherent Two-Dimensional Photocurrent Spectroscopy in a Pbs Quantum Dot Photocell. *Nature communications* **2014,** *5* (1), 5869.

10. Bolzonello, L.; Bernal-Texca, F.; Gerling, L. G.; Ockova, J.; Collini, E.; Martorell, J.; Van Hulst, N. F., Photocurrent-Detected 2d Electronic Spectroscopy Reveals Ultrafast Hole Transfer in Operating Pm6/Y6 Organic Solar Cells. *The Journal of Physical Chemistry Letters* **2021,** *12* (16), 3983-3988.

11. Nardin, G.; Autry, T. M.; Silverman, K. L.; Cundiff, S. T., Multidimensional Coherent Photocurrent Spectroscopy of a Semiconductor Nanostructure. *Optics express* **2013,** *21* (23), 28617-28627.

12. Bian, Q.; Ma, F.; Chen, S.; Wei, Q.; Su, X.; Buyanova, I. A.; Chen, W. M.; Ponseca Jr, C. S.; Linares, M.; Karki, K. J., Vibronic Coherence Contributes to Photocurrent Generation in Organic Semiconductor Heterojunction Diodes. *Nature communications* **2020,** *11* (1), 617.

13. Aeschlimann, M.; Brixner, T.; Fischer, A.; Kramer, C.; Melchior, P.; Pfeiffer, W.; Schneider, C.; Strüber, C.; Tuchscherer, P.; Voronine, D. V., Coherent Two-Dimensional Nanoscopy. *Science* **2011,** *333* (6050), 1723-1726.

14. Uhl, D.; Bangert, U.; Bruder, L.; Stienkemeier, F., Coherent Optical 2d Photoelectron Spectroscopy. *Optica* **2021,** *8* (10), 1316-1324.

15. Bruder, L.; Eisfeld, A.; Bangert, U.; Binz, M.; Jakob, M.; Uhl, D.; Schulz-Weiling, M.; Grant, E. R.; Stienkemeier, F., Delocalized Excitons and Interaction Effects in Extremely Dilute Thermal Ensembles. *Physical Chemistry Chemical Physics* **2019,** *21* (5), 2276-2282.

16. Roeding, S.; Brixner, T., Coherent Two-Dimensional Electronic Mass Spectrometry. *Nature Communications* **2018,** *9* (1), 2519.

17. Bruder, L.; Bangert, U.; Binz, M.; Uhl, D.; Vexiau, R.; Bouloufa-Maafa, N.; Dulieu, O.; Stienkemeier, F., Coherent Multidimensional Spectroscopy of Dilute Gas-Phase Nanosystems. *Nature Communications* **2018,** *9* (1), 4823.

18. Bakulin, A. A.; Silva, C.; Vella, E., Ultrafast Spectroscopy with Photocurrent Detection: Watching Excitonic Optoelectronic Systems at Work. *The journal of physical chemistry letters* **2016,** *7* (2), 250-258.

19. Lott, G. A.; Perdomo-Ortiz, A.; Utterback, J. K.; Widom, J. R.; Aspuru-Guzik, A.; Marcus, A. H., Conformation of Self-Assembled Porphyrin Dimers in Liposome Vesicles by Phase-

Modulation 2d Fluorescence Spectroscopy. *Proceedings of the National Academy of Sciences* **2011,** *108* (40), 16521-16526.

20. Malý, P.; Lüttig, J.; Mueller, S.; Schreck, M. H.; Lambert, C.; Brixner, T., Coherently and Fluorescence-Detected Two-Dimensional Electronic Spectroscopy: Direct Comparison on Squaraine Dimers. *Physical Chemistry Chemical Physics* **2020,** *22* (37), 21222-21237.

21. Tiwari, V.; Matutes, Y. A.; Konar, A.; Yu, Z.; Ptaszek, M.; Bocian, D. F.; Holten, D.; Kirmaier, C.; Ogilvie, J. P., Strongly Coupled Bacteriochlorin Dyad Studied Using Phase-Modulated Fluorescence-Detected Two-Dimensional Electronic Spectroscopy. *Optics express* **2018,** *26* (17), 22327-22341.

22. Mueller, S.; Lüttig, J.; Brenneis, L.; Oron, D.; Brixner, T., Observing Multiexciton Correlations in Colloidal Semiconductor Quantum Dots Via Multiple-Quantum Two-Dimensional Fluorescence Spectroscopy. *ACS nano* **2021,** *15* (3), 4647-4657.

23. Zhou, N.; Ouyang, Z.; Hu, J.; Williams, O. F.; Yan, L.; You, W.; Moran, A. M., Distinguishing Energy-and Charge-Transfer Processes in Layered Perovskite Quantum Wells with Two-Dimensional Action Spectroscopies. *The Journal of Physical Chemistry Letters* **2020,** *11* (12), 4570-4577.

24. McNamee, M. G.; Ouyang, Z.; Yan, L.; Gan, Z.; Zhou, N.; Williams, O. F.; You, W.; Moran, A. M., Uncovering Transport Mechanisms in Perovskite Materials and Devices with Recombination-Induced Action Spectroscopies. *The Journal of Physical Chemistry C* **2023,** *127* (6), 2782-2791.

25. Schröter, M.; Pullerits, T.; Kühn, O., Using Fluorescence Detected Two-Dimensional Spectroscopy to Investigate Initial Exciton Delocalization between Coupled Chromophores. *The Journal of Chemical Physics* **2018,** *149* (11).

26. Kalaee, A. A. S.; Damtie, F.; Karki, K. J., Differentiation of True Nonlinear and Incoherent Mixing of Linear Signals in Action-Detected 2d Spectroscopy. *The Journal of Physical Chemistry A* **2019,** *123* (19), 4119-4124.

27. Kühn, O.; Mančal, T.; Pullerits, T., Interpreting Fluorescence Detected Two-Dimensional Electronic Spectroscopy. *The Journal of Physical Chemistry Letters* **2020,** *11* (3), 838-842.

28. Bruschi, M.; Gallina, F.; Fresch, B., Simulating Action-2d Electronic Spectroscopy of Quantum Dots: Insights on the Exciton and Biexciton Interplay from Detection-Mode and Time-Gating. *Physical Chemistry Chemical Physics* **2022,** *24* (45), 27645-27659.

29. Bruschi, M.; Bolzonello, L.; Gallina, F.; Fresch, B., Unifying Nonlinear Response and Incoherent Mixing in Action-2d Electronic Spectroscopy. *The Journal of Physical Chemistry Letters* **2023,** *14* (30), 6872-6879.

30. Bolzonello, L.; Bruschi, M.; Fresch, B.; van Hulst, N. F., Nonlinear Optical Spectroscopy of Molecular Assemblies: What Is Gained and Lost in Action Detection? *The Journal of Physical Chemistry Letters* **2023,** *14* (50), 11438-11446.

31. Kunsel, T.; Tiwari, V.; Matutes, Y. A.; Gardiner, A. T.; Cogdell, R. J.; Ogilvie, J. P.; Jansen, T. L. C., Simulating Fluorescence-Detected Two-Dimensional Electronic Spectroscopy of Multichromophoric Systems. *The Journal of Physical Chemistry B* **2019,** *123* (2), 394-406.

32. Karki, K. J.; Kringle, L.; Marcus, A. H.; Pullerits, T., Phase-Synchronous Detection of Coherent and Incoherent Nonlinear Signals. *Journal of Optics* **2015,** *18* (1), 015504.

33. Malý, P.; Mueller, S.; Lüttig, J.; Lambert, C.; Brixner, T., Signatures of Exciton Dynamics and Interaction in Coherently and Fluorescence-Detected Four-and Six-Wave-Mixing Two-Dimensional Electronic Spectroscopy. *The Journal of Chemical Physics* **2020,** *153* (14).

34. Perdomo-Ortiz, A.; Widom, J. R.; Lott, G. A.; Aspuru-Guzik, A.; Marcus, A. H., Conformation and Electronic Population Transfer in Membrane-Supported Self-Assembled Porphyrin Dimers by 2d Fluorescence Spectroscopy. *The Journal of Physical Chemistry B* **2012,** *116* (35), 10757-10770.

35. Grégoire, P.; Srimath Kandada, A. R.; Vella, E.; Tao, C.; Leonelli, R.; Silva, C., Incoherent Population Mixing Contributions to Phase-Modulation Two-Dimensional Coherent Excitation Spectra. *The Journal of Chemical Physics* **2017,** *147* (11).

36. Bargigia, I.; Gutiérrez-Meza, E.; Valverde-Chávez, D. A.; Marques, S. R.; Srimath Kandada, A. R.; Silva, C., Identifying Incoherent Mixing Effects in the Coherent Two-Dimensional Photocurrent Excitation Spectra of Semiconductors. *The Journal of Chemical Physics* **2022,** *157* (20).

37. Harel, E.; Engel, G. S., Quantum Coherence Spectroscopy Reveals Complex Dynamics in Bacterial Light-Harvesting Complex 2 (Lh2). *Proceedings of the National Academy of Sciences* **2012,** *109* (3), 706-711.

38. Malý, P.; Mančal, T., Signatures of Exciton Delocalization and Exciton–Exciton Annihilation in Fluorescence-Detected Two-Dimensional Coherent Spectroscopy. *The Journal of Physical Chemistry Letters* **2018,** *9* (19), 5654-5659.

39. López-Ortiz, M.; Bolzonello, L.; Bruschi, M.; Fresch, E.; Collini, E.; Hu, C.; Croce, R.; van Hulst, N. F.; Gorostiza, P., Photoelectrochemical Two-Dimensional Electronic Spectroscopy (Pec2des) of Photosystem I: Charge Separation Dynamics Hidden in a Multichromophoric Landscape. *ACS Applied Materials & Interfaces* **2024**.

40. Massey, S. C.; Ting, P.-C.; Yeh, S.-H.; Dahlberg, P. D.; Sohail, S. H.; Allodi, M. A.; Martin, E. C.; Kais, S.; Hunter, C. N.; Engel, G. S., Orientational Dynamics of Transition Dipoles and Exciton Relaxation in Lh2 from Ultrafast Two-Dimensional Anisotropy. *The Journal of Physical Chemistry Letters* **2019,** *10* (2), 270-277.

41. Ferretti, M.; Hendrikx, R.; Romero, E.; Southall, J.; Cogdell, R. J.; Novoderezhkin, V. I.; Scholes, G. D.; Van Grondelle, R., Dark States in the Light-Harvesting Complex 2 Revealed by Two-Dimensional Electronic Spectroscopy. *Scientific reports* **2016,** *6* (1), 20834.

42. Thyrhaug, E.; Schröter, M.; Bukartė, E.; Kühn, O.; Cogdell, R.; Hauer, J.; Zigmantas, D., Intraband Dynamics and Exciton Trapping in the Lh2 Complex of Rhodopseudomonas Acidophila. *The Journal of Chemical Physics* **2021,** *154* (4).

43. Fidler, A. F.; Singh, V. P.; Long, P. D.; Dahlberg, P. D.; Engel, G. S., Time Scales of Coherent Dynamics in the Light-Harvesting Complex 2 (Lh2) of Rhodobacter Sphaeroides. *The journal of physical chemistry letters* **2013,** *4* (9), 1404-1409.

44. Hess, S.; Feldchtein, F.; Babin, A.; Nurgaleev, I.; Pullerits, T.; Sergeev, A.; Sundström, V., Femtosecond Energy Transfer within the Lh2 Peripheral Antenna of the Photosynthetic Purple Bacteria Rhodobacter Sphaeroides and Rhodopseudomonas Palustris Ll. *Chemical physics letters* **1993,** *216* (3-6), 247-257.

45. Freiberg, A.; Jackson, J.; Lin, S.; Woodbury, N., Subpicosecond Pump− Supercontinuum Probe Spectroscopy of Lh2 Photosynthetic Antenna Proteins at Low Temperature. *The Journal of Physical Chemistry A* **1998,** *102* (23), 4372-4380.

46. Sundström, V.; Pullerits, T.; van Grondelle, R., Photosynthetic Light-Harvesting: Reconciling Dynamics and Structure of Purple Bacterial Lh2 Reveals Function of Photosynthetic Unit. ACS Publications: 1999; Vol. 103, pp 2327-2346.

47. McDermott, G.; Prince, S.; Freer, A.; Hawthornthwaite-Lawless, A.; Papiz, M.; Cogdell, R.; Isaacs, N., Crystal Structure of an Integral Membrane Light-Harvesting Complex from Photosynthetic Bacteria. *Nature* **1995,** *374* (6522), 517-521.

48. Kasha–Vavilov Rule. 3.0.1 ed.; International Union of Pure and Applied Chemistry (IUPAC): 2019.

49. Forster, L. S.; Livingston, R., The Absolute Quantum Yields of the Fluorescence of Chlorophyll Solutions. *The Journal of Chemical Physics* **1952,** *20* (8), 1315-1320.

50. Cherezov, V.; Clogston, J.; Papiz, M. Z.; Caffrey, M., Room to Move: Crystallizing Membrane Proteins in Swollen Lipidic Mesophases. *Journal of Molecular Biology* **2006,** *357* (5), 1605-1618.

51. Novoderezhkin, V. I.; Stuart, T. A. C.; van Grondelle, R., Dynamics of Exciton Relaxation in Lh2 Antenna Probed by Multipulse Nonlinear Spectroscopy. *Journal of Physical Chemistry A* **2011,** *115* (16), 3834-3844.

52. Novoderezhkin, V. I.; Rutkauskas, D.; van Grondelle, R., Dynamics of the Emission Spectrum of a Single Lh2 Complex: Interplay of Slow and Fast Nuclear Motions. *Biophysical Journal* **2006,** *90* (8), 2890-2902.

53. Maly, P.; Gardiner, A. T.; Cogdell, R. J.; van Grondelle, R.; Mancal, T., Robust Light Harvesting by a Noisy Antenna. *Physical Chemistry Chemical Physics* **2018,** *20* (6), 4360-4372.

54. Fidler, A. F.; Singh, V. P.; Long, P. D.; Dahlberg, P. D.; Engel, G. S., Probing Energy Transfer Events in the Light Harvesting Complex 2 (Lh2) of Rhodobacter Sphaeroides with Two-Dimensional Spectroscopy. *The Journal of Chemical Physics* **2013,** *139* (15).

55. Pullerits, T.; Chachisvilis, M.; Sundstrom, V., Exciton Delocalization Length in the B850 Antenna of Rhodobacter Sphaeroides. *Journal of Physical Chemistry* **1996,** *100* (25), 10787-10792.

56. Hess, S.; Feldchtein, F.; Babin, A.; Nurgaleev, I.; Pullerits, T.; Sergeev, A.; Sundström, V., Femtosecond Energy Transfer within the Lh2 Peripheral Antenna of the Photosynthetic Purple Bacteria Rhodobacter Sphaeroides and Rhodopseudomonas Palustris Ll. *Chemical Physics Letters* **1993,** *216* (3), 247-257.

57. Dostál, J., Nonresonant Coherent Two-Dimensional Spectroscopy. *Spectrochimica Acta Part A: Molecular and Biomolecular Spectroscopy* **2022,** *267*, 120441.

58. Yang, J. M.; Gelin, M. F.; Chen, L. P.; Sanda, F.; Thyrhaug, E.; Hauer, J., Two-Dimensional Fluorescence Excitation Spectroscopy: A Novel Technique for Monitoring Excited-State Photophysics of Molecular Species with High Time and Frequency Resolution. *Journal of Chemical Physics* **2023,** *159* (7).

59. Jana, S.; Durst, S.; Lippitz, M., Fluorescence-Detected Two-Dimensional Electronic Spectroscopy of a Single Molecule. *arXiv:2407.09200* **2024**.

60. Song, Y.; Sechrist, R.; Nguyen, H. H.; Johnson, W.; Abramavicius, D.; Redding, K. E.; Ogilvie, J. P., Excitonic Structure and Charge Separation in the Heliobacterial Reaction Center Probed by Multispectral Multidimensional Spectroscopy. *Nature Communications* **2021,** *12* (1), 2801.

61. Konar, A.; Sechrist, R.; Song, Y.; Policht, V. R.; Laible, P. D.; Bocian, D. F.; Holten, D.; Kirmaier, C. R.; Ogilvie, J. P., Electronic Interactions in the Bacterial Reaction Center Revealed by Two-Color 2d Electronic Spectroscopy. *The Journal of Physical Chemistry Letters* **2018,** *9*, 5219-5225.

62. Símová, I.; Kuznetsova, V.; Gardiner, A. T.; Sebelík, V.; Koblízek, M.; Fuciman, M.; Polívka, T., Carotenoid Responds to Excess Energy Dissipation in the Lh2 Complex from *Rhodoblastus Acidophilus*. *Photosynthesis Research* **2022,** *154* (1), 75-87.

63. Tekavec, P. F.; Dyke, T. R.; Marcus, A. H., Wave Packet Interferometry and Quantum State Reconstruction by Acousto-Optic Phase Modulation. *The Journal of chemical physics* **2006,** *125* (19).

64. Myers, J. A.; Lewis, K. L.; Tekavec, P. F.; Ogilvie, J. P., Two-Color Two-Dimensional Fourier Transform Electronic Spectroscopy with a Pulse-Shaper. *Optics express* **2008,** *16* (22), 17420-17428.

65. Tretiak, S.; Middleton, C.; Chernyak, V.; Mukamel, S., Exciton Hamiltonian for the Bacteriochlorophyll System in the Lh2 Antenna Complex of Purple Bacteria. *Journal Of Physical Chemistry B* **2000,** *104* (18), 4519-4528.

66. Cupellini, L.; Caprasecca, S.; Guido, C. A.; Muh, F.; Renger, T.; Mennucci, B., Coupling to Charge Transfer States Is the Key to Modulate the Optical Bands for Efficient Light Harvesting in Purple Bacteria. *Journal of Physical Chemistry Letters* **2018,** *9* (23), 6892-6899.